Z-pinch interferometry analysis with the Fourier-based TNT code

M. P. Valdivia [1,2], G. Pérez-Callejo [3], L. Izquierdo [4], F. Veloso [4], A. Truong [1], H. Hu [1], N. Dilworth [1], S. Bott-Suzuki [1], V. Bouffetier [5,6]

[1]University of California San Diego, La Jolla, California, USA
[2]Physics and Astronomy Department, The Johns Hopkins University, Baltimore, Maryland, USA
[3]Departamento de Física Teórica Atómica y Óptica, Universidad de Valladolid, 47011 Valladolid, Spain
[4]Instituto de Física, Pontificia Universidad Católica de Chile, Santiago, Chile
[5]CELLS - ALBA Synchrotron Light Source, Barcelona, Spain
[6]European XFEL GmbH, Holzkoppel 4, 22869 Schenefeld, Germany

We present the analysis of interferometry diagnostics with the user-friendy Talbot Numerical Tool (TNT), a Fourier-based post-processing code that enables real-time assessment of plasma systems. TNT performance was explored with visible and infrared interferometry in pulsed-power driven Z-pinch configurations to expand its capabilities beyond Talbot X-ray interferometry in the high-intensity laser environment. TNT enabled accurate electron density characterization of magnetically-driven plasma flows and shocks through phase retrieval methods that did not require data modification or masking. TNT demonstrated enhanced resolution, detecting below 4% fringe shift, which corresponds to 8.7$\times10^{15}$ cm^{-2} within 28 μm, approaching the laser probing system limit. TNT was tested against a well-known interferometry analysis software, delivering an average resolving power nearly 10 times better ($\sim$28 μm versus $\sim$210 μm) when resolving plasma ablation features. TNT demonstrated higher sensitivity when probing sharp electron density gradients in supersonic shocks. A maximum electron areal density of 4.1$\times10^{17}$ cm^{-2} was measured in the shocked plasma region and a minimum electron density detection of $\sim$1.0$\times10^{15}$ cm^{-2} was achieved. When probing colliding plasma flows, the calculations of the effective adiabatic index and the associated errors were improved from $\gamma^* = 2.6 \pm 1.6$ to 1.4 ± 0.2 with TNT post-processing, contributing valuable data for the interpretation of radiative transport. Additional applications of TNT in the characterization of pulsed-power plasmas and beyond are discussed.

I. Introduction

Imaging diagnostics are a useful tool to characterize samples with high resolution and sensitivity. Laser probing diagnostics have become a standard diagnostic in pulsed-power systems [1]. Interferometry can provide reliable electron density information of Z-pinch configurations from phase measurements through Fourier methods. Several interferometry post-processing codes and algorithms offer different phase-retrieval capabilities, which must be evaluated carefully to determine their suitability for each application. One such example is the Talbot Numerical Tool (TNT), which enables rapid and accurate phase retrieval in a user-friendly package.

TNT was developed as a sub-module of the Talbot Interferometry Analyzer (TIA) code [2]. While TIA is a user-friendly forward modelling code, designed to generate synthetic X-ray Talbot-Lau Deflectometry interferograms, its last sub-module includes of a series of dedicated routines to post-process and analyze these interferograms using automated Fourier signal processing. Specific features have been integrated to analyze highly-dense plasmas generated by high-intensity lasers. TNT is a standalone version of the TIA post-processing module described, adapted to work with experimental data directly, that is, no forward modelling is required. Moreover, TNT can post-process interferometry data beyond X-ray Moire images, which includes grating phase-scanning analysis methods [3]. TNT has enabled enhanced phase reconstruction accuracy in recent high-intensity laser experiments [4], [5], where steep electron density gradients were resolved with high diagnostic sensitivity.

The TNT code is developed using MatLab [6], a coding language that uses C routines behind its native functions, permitting rapid calculations. The combination of C routines within MatLab functions and Fast Fourier Transform algorithms enables quick image processing of large interferograms, typically delivering transmission, phase shift, and dark field images in under a minute when run on personal computers with standard processing capabilities. Therefore, TNT can support real-time data analysis to experimental campaigns that require quick assessment of results. Moreover, TNT post-processing can be applied to high repetition rate systems and future developments making use of machine learning algorithms can contribute to advanced data analysis capabilities.

TNT is a user-friendly tool, which can be operated within a Graphical User Interface (GUI), making it accessible for users who may not be familiar with the coding environment. In its *automatic* operation mode, TNT requires minimum user input. Once the data images are loaded into the code, TNT will detect the points of maximum intensity in the corresponding Fourier transforms, and associate them to the periodicity of the fringes. It will then select a region around those peaks based on the intensity of the surrounding pixels, and return Fourier components associated to different data features (as detailed further below). Nevertheless, if the user is more experienced and familiar with the techniques of Fourier analysis, TNT also includes a *manual* operation mode, which allows the user to manually select the desired Fourier peaks by specifying the region corresponding to each Fourier component, effectively constraining or relaxing data filtering in the Fourier space. TNT input allows for several data formats to be loaded

Corresponding author: M. P. Valdivia (email: mpvaldivialeiva@ucsd.edu).

and saved beyond the standard 8-bit dynamic range. This feature enables higher resolution recording of interferograms, which can lead to higher diagnostic accuracy since resolution is limited by the amplitude of the phase curve in Fourier processing methods.

TNT offers a comprehensive framework for interferometry data analysis with specific features for x-ray deflectometry. The TNT user interface enables selection of multiple Fourier orders. Peaks can be identified and filtered by the code automatically or manually selected by the user. A full technical report of TNT data analysis algorithms can be found in Pérez-Callejo *et al.* [2]. Nevertheless, a brief summary of the Fourier analysis performed by TNT is presented here.

A periodic fringe pattern $S(x, y)$ can be expressed as [7]:

$$S(x, y) = A(x, y) + B(x, y)e^{i\phi(x,y)}, \tag{1}$$

where (x, y) are the spatial coordinates of a given position in the image, the first term corresponds to non-periodic features related to beam attenuation effects, and the second term is related to the fringe pattern periodicity and any fluctuations therein. ϕ describes the wavefront phase.

The TNT algorithm separates Fourier components such that the main illumination term (A) can be obtained from the 0^{th} order, while the 1^{st} Fourier order yields the term $C = B\ e^{i\phi}$, related to the phase. The separation is achieved by selecting and masking the appropriate peaks in the Fourier space [8], as detailed further in Ref. [4]. By extracting the real and imaginary parts of $\log[C]$, it becomes possible to isolate B and ϕ. This allows TNT to retrieve the amplitude of the wavefront at the detector plane (A) and its phase (ϕ).

Interferometry diagnostics generally require a set of images to account for non-uniform phase profile: a *Reference* image of the unperturbed interference pattern (i.e., freely propagating beam) and an *Object* image in which the fringe pattern is perturbed by the probed sample. Once A, B, and ϕ have been extracted from the Reference and Object images, the phase shift image can be retrieved from:

$$\Delta\phi = \phi_{\text{Obj}} - \phi_{\text{Ref}}, \tag{2}$$

which depicts the phase gradient resulting from the interaction between the wavefront and the sample.

For optical and infrared light, the refractive index n of a plasma can be written as:

$$n = \sqrt{1 - \frac{n_e}{n_c}} \approx 1 - \frac{n_e}{2n_c}, \tag{3}$$

where n_c is the critical electron density as determined by the probing beam wavelength. Note that this approximation is valid for underdense plasmas where $n_e \ll n_c$.

The phase difference between a plasma probing beam and a beam propagating in vacuum ($n = 1$) is given by:

$$\Delta\phi = \frac{2\pi}{\lambda} \int (n - 1) \cdot dl \approx \frac{\pi}{\lambda n_c} \int n_e \cdot dl, \tag{4}$$

where λ is the beam wavelength. Note that the integral is performed along the probing beam direction of propagation. Hence, areal electron density can be obtained from Eqn. 4.

II. TNT ANALYSIS OF PULSED-POWER EXPERIMENTS

Increased diagnostic accuracy can benefit studies related to ablation dynamics [9] as well as the development and evolution of electro-thermal and magneto-Rayleigh-Taylor instabilities [10]. Thus, TNT can play an important role in studies supporting Magnetized-Liner Fusion (MagLIF) [11], [12] experiments, providing increased quality data to better constrain simulation codes and models. Going beyond, x-ray interferometry can probe a new density regime that may offer enhanced electron density gradient resolving power [13], [14].

Typically, interferometry analysis methods require image contrast enhancement, careful selection of specific regions of interest (ROI), and/or masking specific areas within the ROI. Most codes perform a sinusoidal fit to the periodic fringe data, which imposes restrictions related to fringe contrast and intensity levels within the ROI to be processed. This is relevant in Z-pinch experiments, where multiple spark discharges (common in the operation of pulsed power drivers) may affect the background intensity profile. This should be considered in context with acquisition capabilities of the imaging system, in addition to detector quantum efficiency. In contrast, TNT operates directly in Fourier space, by identifying the spatial frequency of the fringes and masking the frequencies directly. This makes TNT particularly powerful when dealing with broken fringes due to non-uniform intensity profiles, a common issue encountered in experimental interferometry data. Note that broken fringes are also highly periodic, and so their signal is encoded in the Fourier transform around the corresponding Fourier peak. This simplifies data processing significantly, since the code does not *follow* fringes, but rather looks at a reduced area in the Fourier space. By comparing the Fourier transform of the probed object and a reference image, absolute fringe deviations are easily obtained. The algorithm is described in more detail in reference [4].

To highlight TNT phase retrieval capabilities for pulsed-power experiments, data analysis from Mach-Zehnder interferometry diagnostics will be presented for two Z-pinch configurations as follows. An exploder wire configuration was probed with an infrared laser system to investigate magnetically-induced plasma currents and shocks. TNT speed and ease of use were first evaluated considering phase-shift reconstruction of raw interferograms. A full experimental view of exploder array features and the interaction region between low-density plasma flow and a solid obstacle is presented. A thorough description of plasma features explores post-processed data accuracy. TNT phase retrieval capabilities are compared with a standard interferometry analysis code to evaluate performance in context of sensitivity and resolution. A second Z-pinch configuration, designed to study the interaction region between a plasma jet generated by a wire array and a laser-produced plasma plume, is presented. A code comparison is presented for areal electron density retrieval. An evaluation of TNT performance is presented considering the ability to resolve important plasma features and obtain accurate measurements relevant to plasma dynamics studies.

III. Plasma Flow and Shock Studies Using Wire Exploder Configuration

Plasma flow and shock dynamics can be investigated in pulsed-power experiments involving a wide variety of Z-pinch configurations [15], [16], [17]. Inverse wire arrays are useful and well-known platforms that enable hydrodynamic flow studies in the High Energy Density regime [18], [19]. Bott-Suzuki *et al.* [20] demonstrated supersonic shock formation (M ∼6) in an exploder wire platform, where a quasi-uniform, large-scale hydrodynamic flow was accelerated by Lorentz forces. These Z-pinch platforms can help determine shock formation conditions and evolution in context of plasma flow dynamics. Coniering that enhanced diagnostic resolution and sensitivity can better highlight specific Z-pinch features (e.g., ablation flares) as well as high density gradient (e.g., shock interaction region), TNT performance was assessed through the analysis of exploder array data.

A. The two-wire exploder: an experimental platform for plasma flow and shock studies

Wire exploder Z-pinch configurations provide a useful platform to study plasma flow dynamics in a simple configuration. In a two-wire exploder, shock formation and evolution is determined by experimental parameters that can be easily controlled or modified, thus enabling systematic studies. The two-wire exploder configuration studied was constructed with 150 μm diameter tungsten wire load and loop obstacle. A schematic can be found in Figure 1 aswell as pictures highlighting electrodes and current monitors.

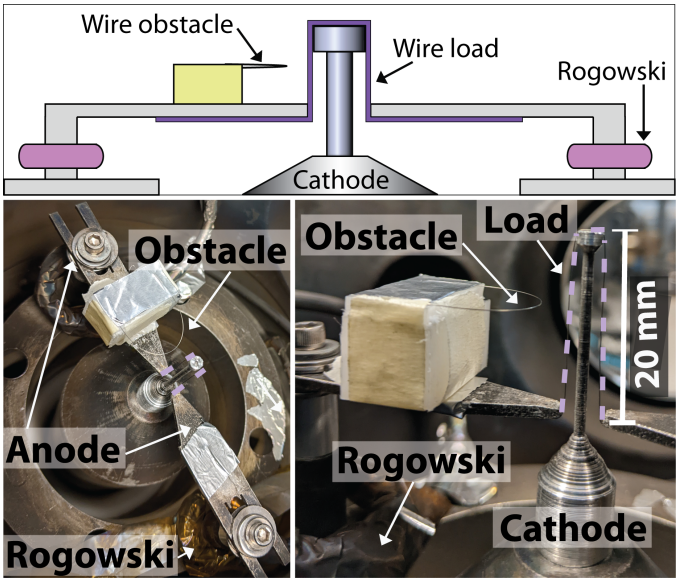

Fig. 1. Wire exploder configuration. Top: Schematic showing load and obstacle wires, electrodes, and current probes. Bottom: Top-down (left) and side-on (right) angled views.

The two-wire exploder was driven by the Bertha pulser (∼200 kA, ∼1.1 μs risetime) [21]. The current flowing through each return post was monitored with two independent Rogowski coils. The total current through the load was calculated from these two measurements. Figure 2 shows the current traces obtained in a typical shot. The total current signal indicates that a peak value of 180.8 kA was reached 1.05 μs after current start. The plot also shows the diode signal that was used to determine diagnostic laser probe start time.

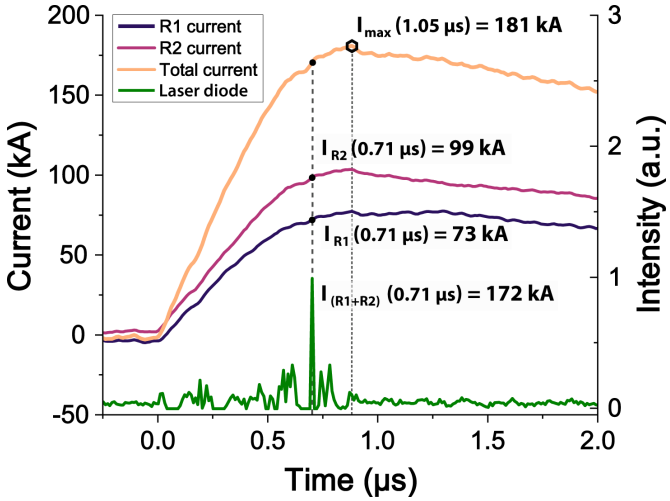

Fig. 2. Current signals from individual Rogowski coil voltages (I_{R1} and I_{R2}) and corresponding total current (I_{R1+R2}). Interferometry timing was given by laser diode signal.

B. Full-view assessment of the plasma system

Plasma dynamics were characterized through time-resolved infrared Mach-Zehnder interferometry (Nd:YAG laser, 1064 nm, 6.5 ns). An interferogram was recorded 0.71 μs after current start, with time resolution given by laser pulse length. Figure 3 shows a color-enhanced version of the image recorded with magnified view insets to better showcase the interference pattern. Note that the period of the interference pattern and its curvature vary within the image and thus, non-uniformity must be considered in data analysis and interpretation.

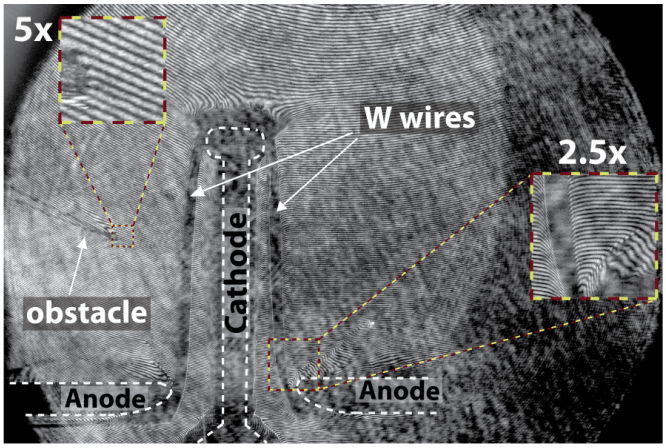

Fig. 3. Interferogram of the two-wire exploder plasma load. Insets show two magnified sections. Image contrast has been modified in this figure for viewing purposes.

Figure 4 presents the data obtained from TNT post-processing of the raw data shown in Fig. 3. In this case,

unaltered images were loaded to TNT and neither masks are employed nor specific areas are selected in the data analysis process. The entire phase retrieval procedure, from image loading to data storage, took less than a minute to complete.[1] Figure 4 presents phase and areal electron density maps generated from interferometry data post-processing of Fig. 3, demonstrating that TNT can efficiently provide a complete view of the probed system without the need to alter the interferometry images.

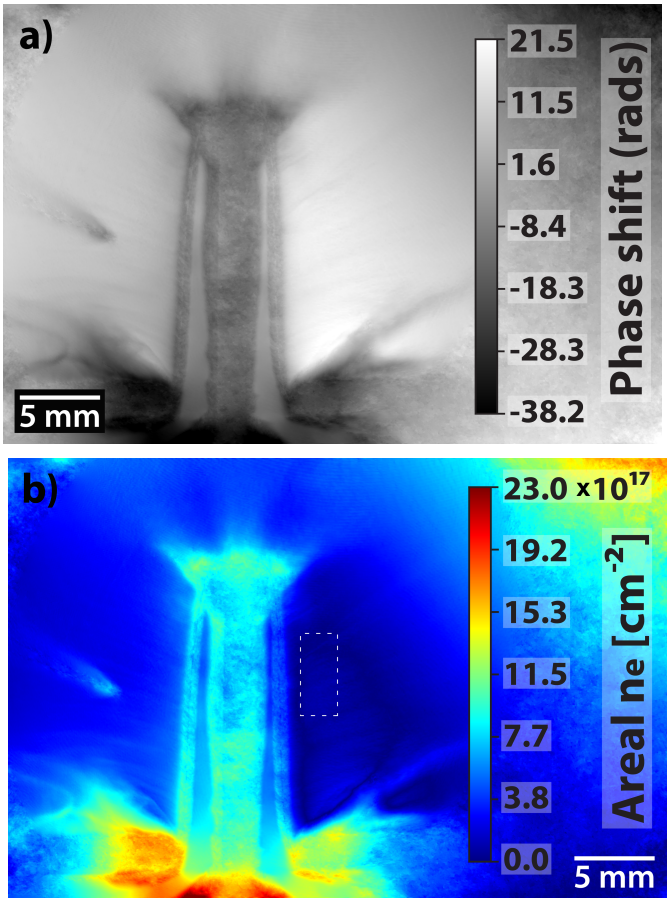

Fig. 4. Results from TNT post-processing of raw interferograms: a) Phase shift and b) corresponding areal electron density color map.

Results shown in Figure 4 demonstrate that the TNT code is robust; it can work with images containing sharp interfaces and heavily attenuating or otherwise solid objects (e.g., electrodes). The latter is especially relevant to data analysis of Z-pinch configurations. Pulsed-power experimental schemes are often constricted by vacuum chamber size and electrode geometry, making diagnostic field of view a challenge. Notably, TNT post-processing did not use masks nor was it necessary to it modify the raw interferogram data in any way, which is not the case for most interferometry analysis codes. While the phase map obtained with TNT shows non-zero values within solid objects (Fig. 4a), disambiguation is possible by inferring electrode and wire locations from reference images. It is understood that the values assigned to electrode and wire locations hold no physical meaning since these areas experience no phase shift. Indeed, said values average to zero within measurement error, noting that this may also serve as means to assess the level of uncertainty associated to the phase maps retrieved. Additional details and further numerical analysis will be presented in a future publication addressing TNT code capabilities and limitations for experimental configurations beyond pulsed-power applications.

[1]As an example, the TNT data analysis takes less than a minute when executed on a Ryzen 7 laptop, with 12GB of RAM, and on an Intel(R) Core(TM) i5-6500 CPU @3.20GHz, with 16GB of RAM.

C. TNT phase retrieval accuracy

Distinctive features of dense Z-pinch dynamics, such as wire expansion and ablation flares, can be identified in the phase shift image obtained through TNT post-processing and its corresponding areal electron density image (Fig. 4b). In wire array systems, wire core heating and expansion are expected as current goes through through the wires. Non-uniform mass ablation is observed along the wires and periodic plasma streams can be identified along their outer surface. These plasma streams carry mass away from the wire. In the experiment, low-density plasma surrounds the wire cores. Wire diameters of 919 $\pm$ 47 μm and 825 $\pm$ 38 μm were determined for the left and right wires, respectively.

The discrepancy in wire expansion is explained by independent current measurements (Fig. 2), where I_{R1} = 99 kA was calculated for the left wire and I_{R2} = 73 kA was calculated for the right wire. In this case, the current flow asymmetry is significant enough to impact plasma dynamics, which may be inferred from the data shown in Figure 4b. According to Z-pinch dynamics [1], [20], higher areal electron densities are expected near the wires. An average areal electron density of $6.01 \pm 0.35 \times 10^{17}$ cm^{-2} was determined for the area surrounding the wires defined by r_{solid} = 75 μm to $r_{expanded}$ = 133 μm (Figure 4b). Assuming axial symmetry around the wire, electron densities above 2.3×10^{20} cm^{-3} were computed for an effective wire radius of $\sim$133 μm. Thus, plasma electron density values $\sim$45% of critical density could be obtained at the wire surface, based on TNT post-processed data.

Note that the accuracy of post-processed interferometry data depends on the ability to distinguish consecutive fringes within the smallest spatial unit.Further, the minimum and maximum detectable fringe shift values are determined by several factors including diagnostic limitations (e.g., critical density, spatial resolution from optical system, and detector dynamic range), probed object properties (e.g., dimensions and composition) and combinations thereof. For example, low and/or non-uniform probe beam intensity can lead to poor fringe contrast, which is detrimental to phase retrieval accuracy. Data analysis codes may address these issues differently. The unique data processing approach provided by TNT has been optimized to achieve high diagnostic sensitivity and resolution. Since TNT works directly in the Fourier space, the resolution limit depends on Fourier peak selection. It is important to note that TNT does not perform sinusoidal fitting, hence, no artificial smoothing is introduced by the phase retrieval algorithm. This has major implications in the quality of data obtained. In combination with highly sensitive diagnostics, the code can detct sub-period fringe shifts with improved data accuracy.

D. Evaluation of phase-retrieval sensitivity

Diagnostic data processing techniques must be optimized to take full advantage of their inherent sensitivity and resolution. Considering the current state of laser-based interferometry diagnostics for Z-pinches, improved data analysis methods were pursued. In the above, it was shown that TNT can easily support quick data processing in systematic studies of Z-pinches. To test TNT performance, a direct comparison of post-processed data quality was made against IDEA [22], a software designed for fringe analysis and phase data reduction that has been widely used by the pulsed-power community. A small region at the center of Figure 3 was selected considering areas with no discernible broken fringes and sufficient signal level where minimum and maximum amplitude could be distinguished within the interference pattern.

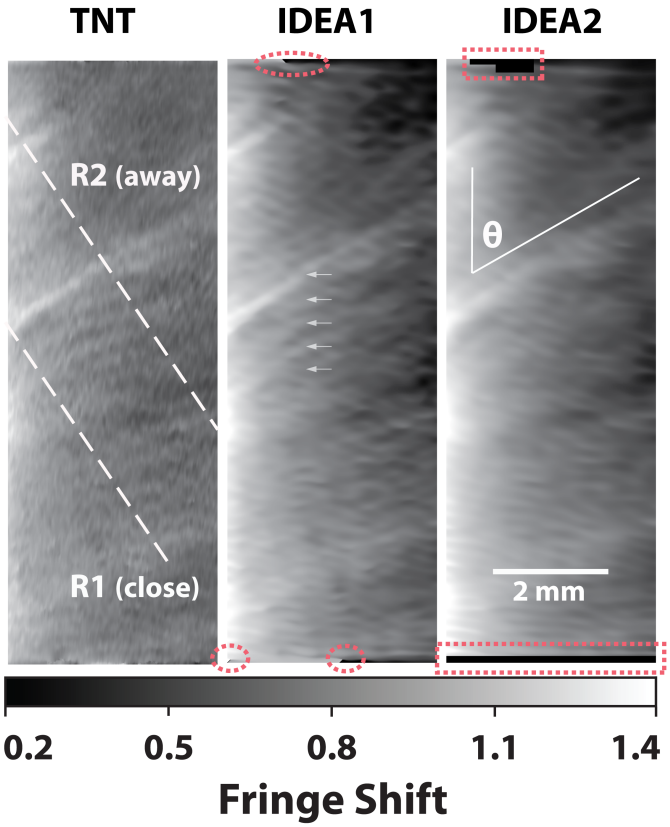

Fig. 5. Fringe shift maps obtained with TNT and IDEA for a small area at the center of Fig. 3. IDEA processing was done for two different masked areas and Fourier peak selections. Line-outs were taken at two radial positions perpendicular to the direction of ablation flare expansion. White dashed lines indicate *R1* and *R2* positions (closer and farther away from the wire, respectively). Periodic ablation flare structures are indicated by arrows and the flow direction is indicated by θ

Figure 5 presents the fringe map obtained from TNT post-processing of cropped raw reference and object image sets of a region showing plasma flow near the wire, indicated by dashed box in Figure 4b. Two different fringe shift maps were retrieved with IDEA using the same interferometry image set. IDEA1 labeling (Fig. 5, center) shows the fringe shift map retrieved using minimum filtration in the Fourier domain to preserve information and maximize resolution. However, the reconstructed image shows three areas that suffered from the so-called 2-Pi uncertainty (red dotted circles), as the algorithm failed to properly identify the corresponding original fringe position in the reference image. As consequence, an over or under estimation equivalent to at least one full fringe period may be expected. IDEA2 indicates a second retrieval in which problem areas were masked within the software (red dotted squares). Increased filtration in the Fourier space was required, leading to resolution loss, as observed when comparing fringe shift maps. Note that masking introduces data loss in the masked region but it does not necessarily solve the 2-Pi uncertainty issue, which is illustrated by ineffective masking at the top of the IDEA1 and IDEA2 images. Moreover, additional data uncertainty is introduced from fringe shift underestimation, evidenced by lower fringe shift values assigned to the regions away from the wire (right).

It is important to consider that, while masking and Fourier space filtration may be performed to overcome 2-Pi uncertainty, this is often detrimental to diagnostic sensitivity due to poor resolution and reduced detection dynamic range. Additionally, optimal region of interest selection depends strongly on user experience with the code. IDEA offers script capabilities that may help with this selection, nevertheless, user expertise is needed to recognize how mask or area selection might produce artificial fringe discontinuities or, in some cases, it may induce new problem regions. Often, the analyzed area must be severely reduced to avoid potential misinterpretations, particularly near edges.

Ablation flare information is typically extracted from radiography diagnostics, a well-established technique in Z-pinch experimental studies [23], [24]. Although radiographs may be useful for certain experimental applications, forward-fitting methods and plasma properties assumptions are required for precise data analysis and electron density retrieval. This motivates further developments in interferometry diagnostic techniques through improved data post-processing methods. Ablation flare structure (indicated by arrows in Fig. 5) was analyzed considering phase shift line profiles averaged over 20 pixels. Line-outs were taken perpendicular to the plasma flow direction, as defined by the angle θ between the ablation flares and the wire, for two different positions, as indicated by thin long white dashed lines in Figure 5.

Ablation flares can be identified from phase shift line-outs (Fig. 5). TNT, IDEA1, and IDEA2 traces are shown in Figure 6. Individual ablation flare position and local density may be inferred from phase shift line-out peaks considering amplitude and width, as these are related to phase change sensitivity and spatial resolution, respectively. Profiles from both radii indicate that TNT enables enhanced diagnostic sensitivity with increased spatial resolution. Several peaks within the TNT line-out cannot be distinguished from IDEA1 and IDEA2 traces. Moreover, when comparing IDEA1 and IDEA2, it is clear that masking ambiguous regions within an image may reduce phase amplitude as well as spatial resolution. Note that masking is often required in IDEA phase unwrapping. In turn, the TNT code can better assess fringe position avoiding masking altogether. With TNT, a minimum fringe shift of $\sim$4%, can be detected within 3 pixels. This is

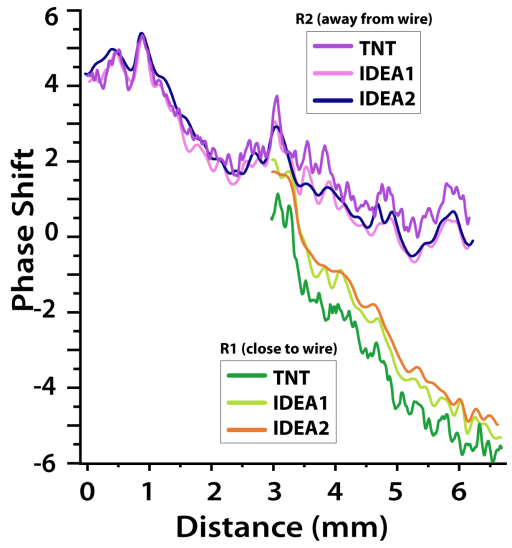

Fig. 6. Line-outs from differential phase shift maps retrieved with TNT and IDEA, corresponding to data from Fig. 5. The plots show ablation flare structures are less prominent away from the wire.

equivalent to an areal electron density lower limit detection of 8.7×10^{15} cm^{-2} (Eqn. 4) within $\sim$28 μm, close to the optical system resolution limit estimate of $\sim$20 μm. In contrast, IDEA line-outs show that 4% fringe shift can be measured within 8 pixels, that is, $\sim$74 μm are required achieve the same level of sensitivity. Recall that these results have higher uncertainty, as shown in Figure 5 and discussed above. Moreover, phase retrieval with IDEA has an associated average resolving power equivalent to 177 μm, here defined as the minimum spatial unit necessary to distinguish two separate peaks. When attempting to overcome the 2-pi uncertainty through data masking and increased Fourier filtering in IDEA, a 5% fringe shift was measured within 13 pixels, which is equivalent to a minimum measurement of 8.7×10^{15} cm^{-2} within $\sim$121 μm. Note that the additional filtering and masking came at the cost of average resolving power, which increased from $\sim$121 μm to 214 μm with IDEA, almost an order of magnitude larger than the average resolving power provided by TNT ($\sim$121 μm).

High density plasma streams, indicated by the arrows in Figure 5, are observed along the wire length and moving radially away from the wires. The well-defined ablation flares have an average wavelength of 209.7 $\pm$ 30.7 μm, determined by sine wave fits of line-outs extracted from TNT phase shift maps and its corresponding error, noting that this value exceeds spatial resolution. In comparison, wavelengths of 0.25 mm were measured by Lebedev *et al.* [15] in a wire array configuration considered to be in the large interwire-gap regime. The results obtained through TNT methods agree with this value when considering statistical error and system resolution.

An areal electron density of $\sim$4.9 $\times10^{16}$ cm^{-2} was determined $\sim$1 mm away from the wire (Figure 5). Note that the small fraction of wire material expanding away from the wires are surrounded by a low-density plasma background, which is below the areal density detection limit of the order of 10^{15} cm^{-2}. The low-density plasma background is easy to distinguish from the ablation flares in the TNT phase map. Note that the ablation structures are more difficult to distinguish far away from the wire. This is explained by a decreasing local magnetic field as plasma moves away from the wire. This results in lower Lorentz force compression. and consequently, lower areal and local electron density. High diagnostic sensitivity is required to accurately resolve these structures, as the density ratio between the plasma streams and the low-density background increases when moving away from the wire. From Figure 5, the low-density plasma background has an areal electron density corresponding to 3-42% of ablation flare mesured values. High diagnostic sensitivity was thus demonstrated, where increased accuracy and phase change sensitivity is achieved with TNT in comparison with IDEA.

E. Resolving steep density gradients with TNT

As mentioned above, accurate plasma flow characterization is relevant to shock studies [20], [19]. In the two-wire exploder configuration, the presence of an obstacle along the path of the ablated plasma flow gives way to a supersonic shock [20], forming a well-defined Mach cone. Therefore, steep density gradients are expected near the wires and the plasma shock. Figure 7 presents a smaller region of interest chosen within Figure 4 to better highlight shock features with TNT post-processing.

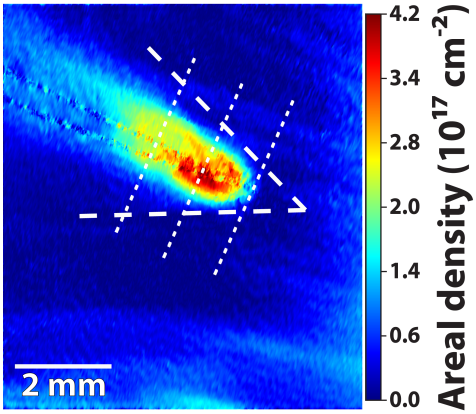

Fig. 7. Shock and plasma flow areal electron density retrieved with TNT. Mach cone opening angle (dash lines) is shown along with areal density line-out positions (dotted lines).

The supersonic shock can be described by the Mach number defined buy the cone aperture. The ablation flare direction determines the Mach cone half opening angle, calculated to be 47.5° $\pm$ 6.2°. Thus, M = 2.48 $\pm$ 0.33 was calculated.

Figure 6 presents areal electron density line-outs taken along the cone's axis of symmetry at three different positions, separated by 1 mm starting at the tip of the obstacle, which were averaged over 50 μm. The three positions are indicated by dashed lines in Figure 7.

The highest areal electron density value was measured 1 mm away from the obstacle, reaching an areal electron density of

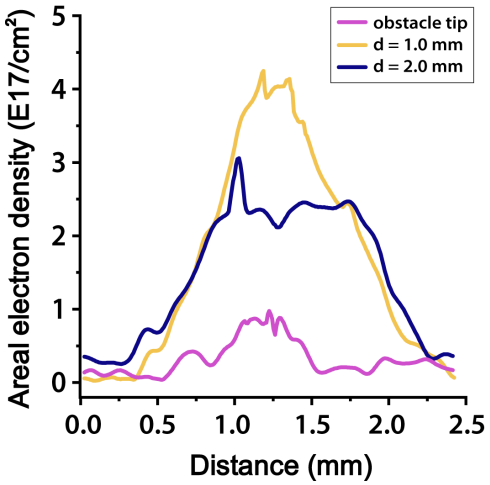

Fig. 8. Areal electron density line-outs taken 0.6, 5.2, and 8.7 mm from the shock front, averaged over 50 μm.

$\sim 4.1\times10^{17}$ cm^{-2}, decaying to a minimum detectable value of $\sim 10^{15}$ cm^{-2} within $\sim$810 μm. These results demonstrate that TNT is capable of high sensitivity probing of sharp electron density gradients, such as those found in supersonic shocks.

IV. Characterization of Conical Wire Array Jet and Plasma Plume Collision

In a recent experiment, collisional shocks were induced through the interaction between a plasma jet emitted by a conical wire z-pinch array and a laser-produced plasma [25]. To understand the physics that governs the interaction region, density measurements are a key element to evaluate the relevance of different plasma processes such as strong radiative cooling or magnetic field compression [26]. For instance, the increase in density due to the shock-mediated interaction can provide valuable information related to the plasma adiabatic index. In addition, the size of the region with augmented density is used as scale length of the interaction region, which is useful when assessing the collisionality regime. Therefore, accurate measurements of electron density with enhanced resolution and sensitivity are crucial.

A. A platform for plasma-plasma interactions

Conical wire arrays have demonstrated production of axial outflows in the form of a collimated plasma jet [27]. Considering a set of dimensionless parameters provided by Euler similarities in magnetohydrodynamics, this plasma jet has been used as a laboratory astrophysics counterpart for Herbig-Haro objects [27], [28]. In order to mimic the interaction of such jets with background plasma ambient, a laser-produced plasma plume was generated in the jet propagation region. This simple configuration gives way to an experimental platform for systematic plasma interaction studies involving two different and separate plasma sources and thus, their density and temperature can be controlled independently.

A conical wire array was driven at $\sim$400 kA in $\sim$350 ns by the Llampudken pulsed-power generator [29] to generate a plasma jet. The conical wire array is composed by 16 equally

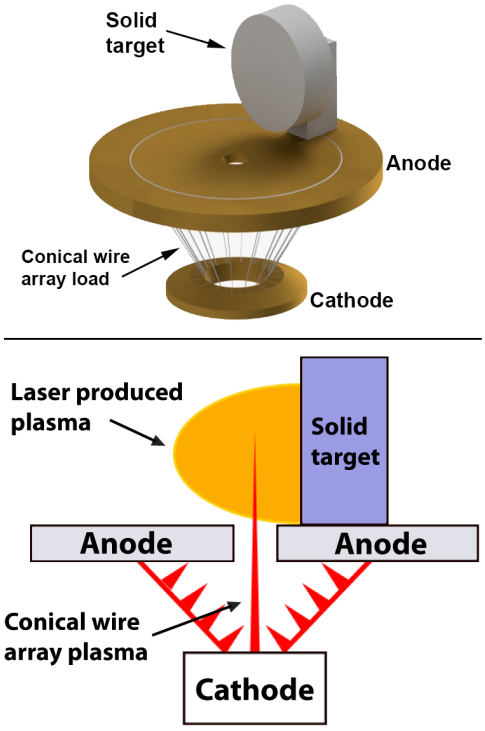

Fig. 9. Plasma-plasma interaction experiment schematic. Top: 3D schematic with no plasma sources. Bottom: 2D representation of conical wire array outflow interacting with a laser-produced plasma plume propagating in the perpendicular from the target.

spaced aluminum wires of 40 μm diameter each and 15 mm length. The array diameters at the cathode and anode are set at 8 and 25 mm, respectively. A flat aluminum target was used to produce a second plasma source. The target was located above the array and perpendicular to the anode, which includes a metallic lid with a 2 mm central hole. The anode design constrains the outflows emission from the array allowing only the jet to propagate upwards. The lid is geometrically designed to avoid direct impact of ablation flares (from the wires in the array) with the aluminium target. At nearly half of the maximum current (t $\sim$200 ns) the target was irradiated by a 80 mJ, 2×10^{10} W/cm^2 laser pulse. The plasma plume generated by the laser-target interaction propagated perpendicular to the plasma jet axis. The conical wire array plasma outflow and the laser-produced plasma front interact in the region above the anode, as shown in Figure 9.

B. Improved plasma adiabatic index determination from TNT phase retrieval

A visible Mach-Zehnder interferometer (6 ns, 532 nm laser) characterized the plasma interaction region. A filtered CMOS camera recorded the interferograms with 8-bit dynamic range and $\sim$4 μm pixel size. The images were processed using IDEA [22], a software that provides spatially resolved phase maps of selected masked areas within an image. To further test TNT phase retrieval processing accuracy, the same interferometry sets were processed using both codes.

Figure 10 presents the color areal density maps obtained by processing the same plasma interaction interferometry data

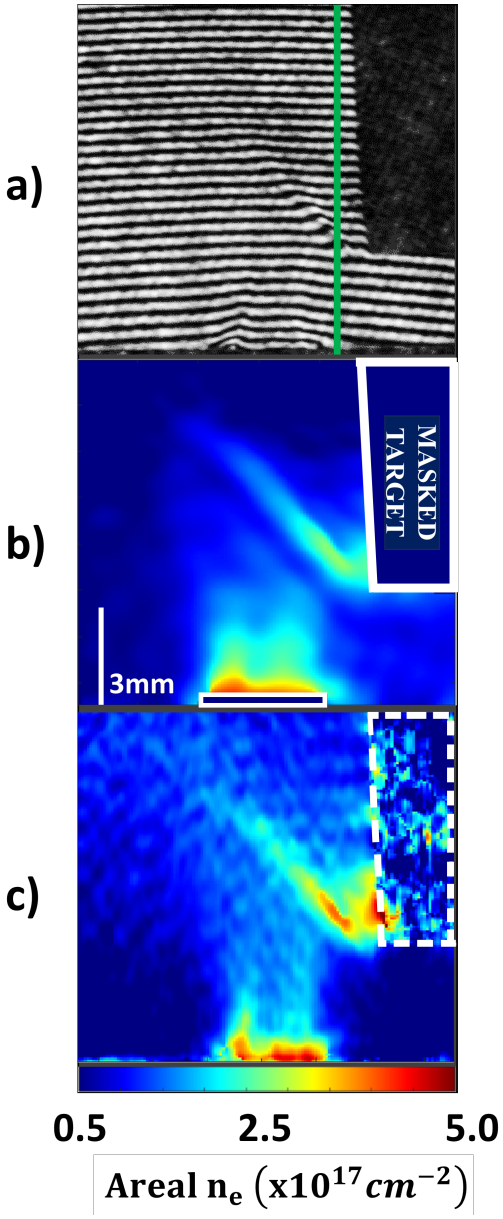

Fig. 10. a) Interferogram of the interaction between a plasma jet and a plasma plume. The green line shows the region where the density jump will be analyzed. Areal plasma density map generated by b) IDEA and c) TNT. The white lines in b) indicate areas that must be masked in IDEA processing. Dashed white lines in c) indicate the unmasked target area.

with IDEA and TNT. The color scales in both images show an increase in areal density in the plasma interaction region. This increase in density is attributed to the formation of a collision-mediated layer. Further details on plasma dynamics and the physics processes involved in the plasma interaction can be found in Ref. [25]. However, in Figure 10 spatial oscillations are observed in the density map, but only for TNT data. Although this is evidence of enhanced TNT phase-retrieval sensitivity, there is no argument to ascribe those variations to real density variations. On the contrary, these are ascribed to irregularities in probing beam intensity distribution. Often, diffraction patterns are produced as the laser propagates through the optical beam path before entering the vacuum chamber, a common occurrence in pulsed-power laser probing. Similarly, IDEA failed to resolve two important regions that are indicated by the red boxes in Figure 10: i) the Z-pinch jet region near the anode (which is also the region of higher density), and ii) the laser-plasma plume near the target.

In IDEA, an adequate mask selection is crucial, otherwise fringe shifts may be either misinterpreted or phase unwrapping cannot be performed altogether. When tight masks were applied to the anode and the target in Figure 10b, the density profiles obtained in the areas surrounding these masks offered incorrect plasma dynamics interpretation. Consequently, masks extended beyond the anode and target surfaces to avoid misinterpretation of spatial changes in plasma density. While more accurate phase unwrapping is achieved, then some information is lost in the vicinity of the masked areas.

Conversely, this issue did not arise in TNT, where phase unwrapping does not require masking of any kind. It is worth noting that, in these opaque regions, TNT will deliver fringe shift values associated to noise, as shown in the dashed white box in Figure 10c. Therefore, phase map interpretation by the user relies on correctly identifying solid and otherwise attenuating objects, where no fringes are present and thus, no fringe shifts are expected. An improved spatial resolution in the interaction region was obtained from the TNT phase shift map. While the interaction zone in Figure 10b exhibits nearly uniform density, TNT reveals a larger density peak in the central region of the interaction zone, closer to the target. Additionally, TNT reveals higher densities near the target, as expected in the laser focus region. The discrepancies between IDEA and TNT results are ascribed to edge effects near masked areas when processing interferogram data with IDEA.

Besides that, Figure 10c shows non-zero density corresponding to a larger area of the laser-produced plasma plume. In this case, the extension of the plasma plume reaches almost the entire width of the image, which is not the case in Figure 10b. This is a direct consequence TNT ability to detect smaller fringe shifts in contrast to IDEA. Since TNT enables the detection of lower densities, a more comprehensive analysis of the laser plasma plume and the position of the interaction region is enabled. The plasma plume size obtained agrees with previous self-emission observations in similar laser plasmas. [30].

A closer analysis of the interaction region was performed using the areal electron density profiles presented in Figure 11, indicated by a green line in Figure 10a. Post-processed data indicate that in the pre-shock region (z<3 mm), the measured areal density is close to the minimum achievable for the diagnostic technique and software capability. This is particularly relevant when evaluating the density increase induced by the shock using the dimensionless quantity $\Omega = \int n_e^{postshock} dl / \int n_e^{preshock} dl$, which provides information on the effective adiabatic index γ^* of the plasma [26]. With a minimum detectable fringe shift of $\sim$12.5% for IDEA phase unwrapping, a density increase of $\Omega = 2.2 \pm 1.3$ is obtained, indicating an effective adiabatic index of $\gamma^*_{IDEA} = 2.6 \pm 1.6$. With this large uncertainty, it is not possible to properly assess the physical processes occurring in the shock. On the contrary,

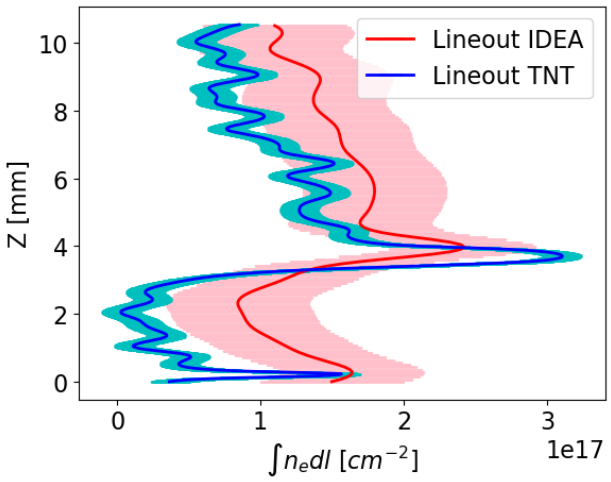

Fig. 11. Areal electron density lineout measured for both images in the same region. Shaded areas correspond to error associated to minimum fringe shift resolution.

the minimum detectable fringe shift of $\sim 4\%$ was determined for TNT post-processed data, providing a density increase of $\Omega = 5.5 \pm 1.6$, corresponding to $\gamma^*_{TNT} = 1.4 \pm 0.2$. Note that the variation in adiabatic index calculations, as determined by each method, significantly alters the interpretation of the physics within the interaction region. The interpretation of radiative transport is challenging when considering shock layer adiabatic index calculations from IDEA. On the other hand, the TNT method enables higher precision, leading to the determination that the shock layer is predominantly radiative and is primarily influenced by radiation [26]. This observation can be complemented by additional diagnostics, such as self-emission images, which will be explored in future publications.

V. Discussion / Summary

We presented applications of a post-processing tool for interferometry diagnostics in the visible and IR domain to study pulsed-power driven plasmas. Electron density mapping of plasma interactions was performed for two Z-pinch configurations: i) supersonic shocks from exploder wires and ii) collision between a plasma jet from a conical wire array and an ablating plasma front from laser-target interaction.

High diagnostic precision was achieved with TNT analysis when investigating the development of magnetically-induced and laser-produced plasmas. Ablation structures were characterized with improved resolution, stemming from high diagnostic sensitivity coupled with advanced phase retrieval numerical methods provided by TNT. This is especially relevant when considering that ablation flare wavelength is typically extracted from radiography [23], [24]. Extracting precise areal electron density from propagation-based radiography diagnostics is challenging as forward-fitting methods and plasma opacity assumptions are required. In turn, refraction-based imaging offers a direct way to determine density gradients through phase shift measurements, as shown in the above.

TNT processing shows higher sensitivity to spatial variations when compared to a standard interferometry analysis tool widely used in the pulsed-power community. The superior diagnostic sensitivity and resolution enabled by TNT led to increased accuracy in the determination of important plasma parameters such as the effective adiabatic index. Considering that accurate areal electron density mapping is seldom obtained from interferometry data due to phase-retrieval limitations, this is an important outcome. Even when phase-retrieval with current interferometry analysis tools is possible, those rarely take full advantage of the diagnostic system capabilities. The versatility and robustness of TNT data analysis can address this long-standing limitation in Z-pinch diagnostics, which stands to benefit pulsed-power research and the plasma community at large.

We presented TNT as a user-friendly tool for accurate interferometry analysis that optimizes diagnostic sensitivity and resolution. Rapid phase retrieval and in-situ assessment capabilities were demonstrated. Notably, the ability to quickly obtain a global areal electron density picture in real time can be extremely helpful during experimental campaigns. Efficient assessment of plasma conditions can inform parameter changes needed to achieve experimental goals in a timely fashion. This unique TNT feature may support high repetition rate experiments requiring fast data analysis with high accuracy, Beyond, this capability can potentially contribute to machine learning schemes, which will further increase diagnostic data processing speed and provide bulk experimental data necessary to benchmark simulation codes, for example. Further details and technical descriptions of TNT code capabilities will be discussed in a future publication presenting in depth comparisons of TNT performance against several interferometry data analysis tools in the analysis of x-ray and optical interferometry data from various platforms.

VI. Acknowledgements

Funding and support to develop and benchmark the TNT code was provided by the US Department of Energy - National Nuclear Security Administration - High Energy Density Laboratory Plasmas Grant Nos. DE-NA0001835, DE-NA0002955, DE-NA0003882, and DE-NA0004028. The work presented was also supported by Research Grants No. PID2019-108764RB-I00 and PID2022-137632OB-I00 from the Spanish Ministry of Science and Innovation and the Conseil Régional Aquitaine (INTALAX) and the Agence Nationale de la Recherche (ANR- 10-IDEX-03-02, ANR-15-CE30-0011), France. Wire exploder work was supported in part by the NNSA SSAA under DOE Cooperative agreement DE-FC03-02NSA00057 and the NNSA SSAP under DOE Cooperative Agreement DE-NA0004148. Plasma-plasma interaction studies were supported by the Agencia Nacional de Investigacion y Desarrollo (ANID) grants of the Gobierno de Chile: ANID-FONDECYT-Regular 1231286 and ANID-Quimal-190011. L.I. also acknowledges funding from ANID-Doctorado Nacional/2023-21230431 grant.

References

[1] M. Haines, "Review of the z-pinch," in *AIP Conference Proceedings*, vol. 345, pp. 254–262, American Institute of Physics, 1995.

[2] G. Pérez-Callejo, V. Bouffetier, L. Ceurvorst, T. Goudal, M. P. Valdivia, D. Stutman, and A. Casner, "TIA: A forward model and analyzer for talbot interferometry experiments of dense plasmas," *Physics of Plasmas*, vol. 29, no. 4, 2022.

[3] M. P. Valdivia, D. Stutman, C. Stoeckl, C. Mileham, I. A. Begishev, J. Bromage, and S. P. Regan, "Talbot-lau x-ray deflectometry phase-retrieval methods for electron density diagnostics in high-energy density experiments," *Appl. Opt.*, vol. 57, pp. 138–145, Jan 2018.

[4] G. Pérez-Callejo, V. Bouffetier, L. Ceurvorst, T. Goudal, S. R. Klein, D. Svyatskiy, M. Holec, P. Perez-Martin, K. Falk, A. Casner, T. E. Weber, G. Kagan, and M. P. Valdivia, "Phase imaging of irradiated foils at the omega ep facility using phase-stepping x-ray talbot–lau deflectometry," *High Power Laser Science and Engineering*, vol. 11, p. e49, 2023.

[5] M. P. Valdivia, G. Pérez-Callejo, V. Bouffetier, G. W. Collins, C. Stoeckl, T. Filkins, C. Mileham, M. Romanofsky, I. A. Begishev, W. Theobald, S. R. Klein, M. K. Schneider, F. Beg, C. Casner, and D. Stutman, "Current advances on talbot–lau x-ray imaging diagnostics for high energy density experiments," *Review of Scientific Instruments*, vol. 93, no. 11, 2022.

[6] MATLAB, *version 9.10.0 (R2021a)*. Natick, Massachusetts: The MathWorks Inc., 2021.

[7] M. Takeda, H. Ina, and S. Kobayashi, "Fourier-transform method of fringe-pattern analysis for computer-based topography and interferometry," *JosA*, vol. 72, no. 1, pp. 156–160, 1982.

[8] M. Seifert, M. Gallersdörfer, V. Ludwig, M. Schuster, F. Horn, G. Pelzer, J. Rieger, T. Michel, and G. Anton, "Improved reconstruction technique for moiré imaging using an x-ray phase-contrast talbot–lau interferometer," *Journal of Imaging*, vol. 4, no. 5, p. 62, 2018.

[9] A. J. Harvey-Thompson, S. V. Lebedev, G. Burdiak, E. M. Waisman, G. N. Hall, F. Suzuki-Vidal, S. N. Bland, J. P. Chittenden, P. De Grouchy, E. Khoory, L. Pickworth, J. Skidmore, and G. Swadling, "Suppression of the ablation phase in wire array z pinches using a tailored current prepulse," *Phys. Rev. Lett.*, vol. 106, p. 205002, May 2011.

[10] J. Pecover and J. Chittenden, "Instability growth for magnetized liner inertial fusion seeded by electro-thermal, electro-choric, and material strength effects," *Physics of Plasmas*, vol. 22, no. 10, 2015.

[11] R. D. McBride, S. A. Slutz, C. A. Jennings, D. Sinars, M. E. Cuneo, M. Herrmann, R. W. Lemke, M. Martin, R. A. Vesey, K. Peterson, *et al.*, "Penetrating radiography of imploding and stagnating beryllium liners on the z accelerator," *Physical review letters*, vol. 109, no. 13, p. 135004, 2012.

[12] M. R. Gomez, S. A. Slutz, A. B. Sefkow, D. B. Sinars, K. D. Hahn, S. B. Hansen, E. C. Harding, P. F. Knapp, P. F. Schmit, C. A. Jennings, *et al.*, "Experimental demonstration of fusion-relevant conditions in magnetized liner inertial fusion," *Physical review letters*, vol. 113, no. 15, p. 155003, 2014.

[13] M. Valdivia, D. Stutman, C. Stoeckl, W. Theobald, C. Mileham, I. Begishev, J. Bromage, and S. Regan, "An x-ray backlit talbot-lau deflectometer for high-energy-density electron density diagnostics," *Review of Scientific Instruments*, vol. 87, no. 2, 2016.

[14] M. P. Valdivia, G. W. Collins IV, F. Conti, and F. Beg, "Wire, hybrid, and laser-cut x-pinches as talbot–lau backlighters for electron density diagnostics," *Plasma Physics and Controlled Fusion*, vol. 64, no. 3, p. 035011, 2022.

[15] S. Lebedev, F. Beg, S. Bland, J. Chittenden, A. Dangor, M. Haines, K. Kwek, S. Pikuz, and T. Shelkovenko, "Effect of discrete wires on the implosion dynamics of wire array z pinches," *Physics of Plasmas*, vol. 8, no. 8, pp. 3734–3747, 2001.

[16] S. C. Bott, D. M. Haas, Y. Eshaq, U. Ueda, R. E. Madden, G. W. Collins, and F. N. Beg, "Ablation studies of low-number wire arrays at $200kA$ using a linear transformer driver," *IEEE transactions on plasma science*, vol. 38, no. 4, pp. 567–573, 2009.

[17] S. C. Bott, D. Mariscal, K. Gunasekera, J. Peebles, F. N. Beg, D. A. Hammer, B. Kusse, J. Greenly, T. Shelkovenko, S. Pikuz, *et al.*, "Experimental analysis of the acceleration region in tungsten wire arrays," *IEEE Transactions on Plasma Science*, vol. 40, no. 12, pp. 3324–3328, 2012.

[18] A. Harvey-Thompson, S. Lebedev, S. Bland, J. Chittenden, G. Hall, A. Marocchino, F. Suzuki-Vidal, S. Bott, J. Palmer, and C. Ning, "Quantitative analysis of plasma ablation using inverse wire array z pinches," *Physics of Plasmas*, vol. 16, no. 2, 2009.

[19] J. L. Peebles, S. C. Bott, K. Gunasekera, J. Kim, L. Harpster, B. Evans, D. Gomez, O. Paran, C. Peterson, and F. N. Beg, "Examination of bow-shock formation in supersonic radiatively cooled plasma flows," *IEEE Transactions on Plasma Science*, vol. 39, no. 11, pp. 2422–2423, 2011.

[20] S. Bott-Suzuki, L. Caballero Bendixsen, S. Cordaro, I. Blesener, C. Hoyt, A. Cahill, B. Kusse, D. Hammer, P. Gourdain, C. Seyler, *et al.*, "Investigation of radiative bow-shocks in magnetically accelerated plasma flows," *Physics of Plasmas*, vol. 22, no. 5, 2015.

[21] J. T. Banasek, T. G. Oliver, S. W. Cordaro, and S. C. Bott-Suzuki, "Free space thomson scattering to study high energy density shocks," *Review of Scientific Instruments*, vol. 92, no. 9, 2021.

[22] M. Hipp, J. Woisetschläger, P. Reiterer, and T. Neger, "Digital evaluation of interferograms," *Measurement*, vol. 36, no. 1, pp. 53–66, 2004.

[23] S. Lebedev, F. Beg, S. Bland, J. Chittenden, A. Dangor, M. Haines, M. Zakaullah, S. Pikuz, T. Shelkovenko, and D. Hammer, "X-ray backlighting of wire array z-pinch implosions using x pinch," *Review of Scientific Instruments*, vol. 72, no. 1, pp. 671–673, 2001.

[24] M. Schollmeier, P. Knapp, D. Ampleford, E. Harding, C. Jennings, D. Lamppa, G. Loisel, M. Martin, G. Robertson, J. Shores, *et al.*, "A 7.2 kev spherical x-ray crystal backlighter for two-frame, two-color backlighting at sandia's z pulsed power facility," *Review of Scientific Instruments*, vol. 88, no. 10, 2017.

[25] L. Izquierdo, F. Veloso, J. Valenzuela, M. Escalona, D. Oportus, and M. Favre, "Shock interactions between plasma jets from conical wire array z-pinches and laser-produced plasma plume," *Results in Physics*, vol. 37, p. 105476, 2022.

[26] R. P. Drake and R. P. Drake, *Introduction to high-energy-density physics*. Springer, 2006.

[27] D. J. Ampleford, S. V. Lebedev, S. N. Bland, S. C. Bott, J. P. Chittenden, C. A. Jennings, V. L. Kantsyrev, A. S. Safronova, V. V. Ivanov, D. A. Fedin, P. J. Laca, M. F. Yilmaz, V. Nalajala, I. Shrestha, K. Williamson, G. Osborne, A. Haboub, and A. Ciardi, "Dynamics of conical wire array Z-pinch implosions," *Physics of Plasmas*, vol. 14, no. 10, p. 102704, 2007.

[28] S. V. Lebedev, A. Frank, and D. D. Ryutov, "Exploring astrophysics-relevant magnetohydrodynamics with pulsed-power laboratory facilities," *Rev. Mod. Phys.*, vol. 91, p. 025002, Apr 2019.

[29] H. Chuaqui, E. Wyndham, C. Friedli, and M. Favre, "Llampüdkeñ: A high-current, low-impedance pulser employing an auxiliary exponential transmission line," *Laser and Particle Beams*, vol. 15, no. 2, pp. 241–248, 1997.

[30] S. Gurlui, M. Agop, P. Nica, M. Ziskind, and C. Focsa, "Experimental and theoretical investigations of a laser-produced aluminum plasma," *Physical Review E*, vol. 78, no. 2, p. 026405, 2008.